The fate of graphene on copper: Intercalation / de-intercalation processes and the role of silicon

Tim Kratky [a,b], Paul Leidinger [a,b,1], Patrick Zeller [a,b,c,2], Jürgen Kraus [a,b], Francesca Genuzio [d,3], Matteo Jugovac [d], Alessandro Sala [d,3], Tevfik Onur Menteş [d], Andrea Locatelli [d], Sebastian Günther [a,b,*]

[a] Technical University of Munich (TUM), Department of Chemistry, Physical Chemistry with Focus on Catalysis, Lichtenbergstr 4, Garching, 85748, Germany
[b] Catalysis Research Center, Ernst-Otto-Fischer-Str. 1, 85748, Garching, Germany
[c] Fritz-Haber Institute, Max-Planck-Society, Dept. Inorganic Chemistry, Faradayweg 4–6, 14195, Berlin, Germany
[d] Elettra-Sincrotrone Trieste S.C.p.A., S.S. 14 - km 163,5 in Area Science Park, 34149, Basovizza, Trieste, Italy

A R T I C L E   I N F O

A B S T R A C T

Intercalation and de-intercalation processes below graphene (g) grown by chemical vapor deposition (CVD) on Cu foils (g/Cu) were investigated in a combined low-energy electron microscopy and X-ray photoemission electron microscopy study. Exposure of g/Cu to air induces oxygen and water intercalation which can be removed by annealing in vacuum leading to clean and well-ordered graphene on Cu. However, prolonged air exposure leads to intercalation of large amounts of oxygen, most likely inducing the formation of copper oxides. If sufficient intercalated oxygen remains at the interface when exceeding 320 °C, graphene is oxidized and burned off. Cu foils can be loaded with silicon on purpose during foil pre-treatment or accidently during long growth time when applying high temperatures at elevated H_2 pressure inducing the reactive removal of Si species from the quartz reactor wall. Due to the dissolution of Si in the Cu bulk, the Si surface concentration remains below detection limit and graphene of equal crystalline quality is grown as if the Cu foil was silicon-free. However, oxygen intercalation underneath graphene on Si-containing Cu foils can induce Si segregation towards the surface and formation of intercalated silica without attacking the covering graphene. Even at high temperatures, segregating Si acts as oxygen scavenger so that graphene resists oxidation. The observed effect explains the usefulness of certain synthesis protocols and paves the way towards large-scale fabrication of electronically decoupled graphene. The effect can be used to immobilize adsorbing oxygen at the interface and image the initial steps of intercalation below graphene *in-situ*.

1. Introduction

Soon after the successful preparation of single-layer graphene by micromechanical cleavage of highly ordered pyrolytic graphite in 2004 [1], epitaxial graphene growth was considered a potential alternative synthesis strategy capable of mass-scale production [2]. In particular, chemical vapor deposition (CVD) on transition metal supports and also epitaxial growth on SiC(0001) were identified as promising preparation protocols [3–5]. Among these methods, graphene CVD growth on Cu

was considered as ideal synthesis route already in 2009 since the growth seemed to be self-limiting after the formation of a single graphene layer [6]. Since then, graphene growth on copper has attracted tremendous interest in trying to identify the best CVD synthesis protocol for the formation of single crystalline, single-layer thick graphene (SLG) [7–9].

Cu foil pre-treatments were investigated to achieve large single crystalline graphene flakes, aiming at suppressing the flake nucleation during CVD growth in order to obtain fewer but larger flakes. This was accomplished either by removing dissolved carbon from the Cu foil [10],

by passivating active sites before actual CVD growth [11] or by implementing two-step CVD growth processes [12]. Also, protocols were tested that do not limit the flake nucleation but favor the growth of flakes with the graphene lattice aligned with respect to each other so that a single crystalline film emerges through seamless stitching of the coalescing flakes [13,14]. A prerequisite of this approach is the conversion of the polycrystalline Cu support into a highly (111)-textured foil [13,15,16], which facilitates the alignment of the growing graphene layer along the densely packed direction of the Cu(111) lattice. The growth of graphene flakes in aligned registry was reported to be favored on (111)-textured Cu foils with highly indexed facets produced by thermal strain engineering [17]. Meanwhile, fundamental insight into the thermodynamics and kinetics of graphene growth on Cu has been gained, and the outcome of CVD growth can be predicted at high precision [18,19], which means that graphene synthesis itself is understood to a great extent. Currently, synthesis protocols are explored on NiCu alloy supports [18] which might be used to lower the temperature during CVD synthesis and reduce the amount of wrinkle formation in the grown layer [19].

Although having established a reliable CVD graphene growth protocol, it was questioned whether the synthesized graphene can be regarded as a material with predictable properties. It turned out that the interaction of graphene with the Cu substrate is a key aspect, e.g., affecting electronic doping and mechanical straining of the grown layer. Raman spectroscopy helped to disentangle both effects with spatial resolution. Mapping a region of interest while acquiring spectral data and plotting the energy dispersion of the G-band versus the one of the 2D-band was used to image electronically doped and mechanically strained areas in the grown film [20]. The level of mechanical strain release and electronic doping was shown to be affected by the thermal treatment of the sample. In a later, similar Raman study, the strain release was related to the formation of Cu oxide under the covering graphene [21]. Angle-resolved photoelectron spectroscopy also addressed the question of whether CVD-grown graphene on Cu is doped, and it was found that the level of doping changed with temperature by affecting the level of oxygen intercalation underneath graphene [22]. Later, *in-situ* X-ray photoelectron spectroscopy (XPS) studies proved that intercalation/de-intercalation of oxygen indeed modifies the graphene doping level in a semi-reversible way [23,24]. It was also noticed that the graphene-substrate interaction strength can be lowered by controlled oxygen intercalation [25] or oxygen-assisted water intercalation underneath graphene [26].

Investigating the detachment of graphene from Cu due to oxide formation raises the question of whether graphene acts as a protective layer against Cu oxidation. While there was consensus on the protective effect of graphene during ambient exposure at short time scales, there has been a debate on the effects following long-term exposures, especially when water was present in the gas-phase environment [27,28]. Meanwhile, intercalation/de-intercalation studies showed that surface chemistry below graphene strongly depends on the fact whether graphene can be lifted from the substrate along flake edges. The effect was observed when intercalating metals below graphene [29] or when opening lateral intercalation channels for reactants in a catalytic reaction [30]. In addition, vertical intercalation through the graphene layer was studied in recent theoretical work [31,32].

Intercalation/de-intercalation properties of synthesized graphene on Cu (g/Cu) are also connected to the presence of silicon in the system which is introduced in hot wall reactors. These reactor types typically use a quartz glass tube as reaction vessel, in which flat quartz supports are often used as carriers for the Cu foil. After performing the graphene synthesis by applying certain CVD conditions in such hot wall reactors, Si-containing particles were found on the Cu foil. These particles were considered responsible for the unwanted formation of defects in the graphene film and/or for the nucleation of graphene islands during CVD growth [33]. In other cases, Si particles were observed that surrounded already grown flakes [34]. The presence of Si on g/Cu was either related

to a potential Si impurity of the used Cu foil [35], or it was shown to originate from Si release from the quartz reactor wall [36–40]. The assignment of Si release from the quartz wall during CVD is in accordance with the known hydrogen-induced release of SiO from fused silica [41]. In most studies, the identified silicon particles were shown to deteriorate the quality of the grown graphene and in all mentioned studies, the amount of silicon released from the quartz tube was large. Thus, several ways trying to lower the amount of Si-based defects were reported [39,40].

In this low energy electron microscopy (LEEM) study, we demonstrate that the release of Si from the reactor wall, its accumulation in the surface near region of the Cu foil underneath graphene and its protective effect against graphene oxidation are interconnected. The effect is subtle, but the presence of Si in the Cu foil determines whether CVD-grown graphene is resistant to oxidation and whether graphene can readily decouple from Cu or not. Note that oxygen intercalation takes place after CVD synthesis when the g/Cu sample is removed from the reactor and exposed to air, i.e., prior to analysis by any further characterization technique. Depending on the duration of the exposure and depending on the Si content of the Cu foil, the further intercalation/de-intercalation behavior of CVD-grown graphene differs. Our findings indicate that the beneficial effect ascribed to certain graphene synthesis recipes has to be reconsidered.

2. Experimental section

Graphene was synthesized on 25 μm thick Cu foils (Alpha Aesar 99.8 % purity) by CVD in a home-built quartz tube reactor, which is described elsewhere [42]. The synthesis recipe consisted of several treatment steps: The temperature ramping of the Cu-loaded reactor in pure hydrogen, or in a hydrogen or argon atmosphere to which a low oxygen partial pressure ($p(O_2) < 10^{-3}$ mbar) was added. During the subsequent pre-treatment in an Ar: O_2 mixture, any carbon-based impurities present in the Cu foil were removed by oxidation. For several experiments, the Cu foils were enriched with Si on purpose before CVD synthesis of the graphene film. The Si enrichment was induced by high-pressure hydrogen exposure at $p(H_2) = 300$ mbar and temperatures above 1045 °C. When exposing to such a high hydrogen pressure, the Si loading was greatly diminished at T ≤ 950 °C as shown in Fig. 1, which indicates that Si release, diffusion and segregation are highly thermally activated processes. However, during foil pre-treatment or CVD growth at T > 1000 °C, Si enrichment of the Cu foil is avoided when restricting the hydrogen exposure to $p(H_2)$ well below 50 mbar. This was the case for the experiments with Si-free Cu foils shown in Figs. 2–4, in contrast to the ones shown in Figs. 5 and 6 where Cu foils were loaded with Si on purpose.

The actual CVD synthesis was performed in a reactive $CH_4:H_2$ atmosphere. The applied synthesis conditions for each sample are listed in the Supplementary information. The samples were removed from the reactor and exposed to air for a given time before being stored in a vacuum suitcase prior to spectro-microscopic characterization.

The experiments were conducted with the spectroscopic photoemission and low energy electron microscope (SPELEEM) instrument in operation at the Nanospectroscopy beamline of the Elettra synchrotron. This microscope allows data acquisition in various operation modes such as low-energy electron microscopy (LEEM), area-selective low-energy electron diffraction (LEED) and x-ray photoemission electron microscopy (XPEEM) as described elsewhere [43,44]. In LEEM, an irradiating electron beam illuminates a surface along the surface normal and the specularly reflected beam is used for the formation of a real space image which changes contrast when varying the so-called start voltage (STV), i.e., a bias voltage between irradiating electron source and sample. Electrons starting at a bias too low to overcome the potential barrier of the sample are reflected in front of the surface which is why this imaging mode is called mirror electron microscopy (MEM). In case that the start voltage is high enough, electrons can overcome the work function

barrier enter the solid and interact with the surface instead of being reflected in front of it. The transition is called the MEM-LEEM transition which is used as reference level for the conversion of the STV into the electron kinetic energy. In MEM, the surface interaction with the irradiating electrons is greatly reduced but the contrast is difficult to interpret which applies especially for g/Cu because essentially three different effects contribute. First, lateral changes in the work function of the sample can be imaged at STV close to the MEM-LEEM transition as electrons are reflected in front of areas with high work function barrier (bright), whereas electrons enter the solid at areas with low work functions and are reflected less effectively (dark). Of course, if the MEM-LEEM transition voltage changes with respect to the start voltage, the contrast changes accordingly. The second contrast mechanism results from the electric field variation in front of a surface that deviates from a perfectly flat plane, which applies to wrinkles in the graphene layer. Thus, wrinkles sticking out of the surface are readily observed in MEM and LEEM and appear as bright or dark lines depending on the focus. The last contrast effect at very low electron energies results from quantum oscillations observed in the electron reflectivity curve of graphene in the energy range between 0 and 5 eV above the MEM-LEEM transition. These oscillations are observed in a LEEM I(V) data set which consists of real space images recorded as a function of the STV, measuring the local electron reflectivity of the (0,0) beam (specularly reflected beam along the optical axis of the microscope). By extracting the image intensity of a selected area and plotting versus the applied STV, spatially resolved I(V)-curves are derived that show characteristic oscillations at low energy [45,46]. The oscillations allow to identify the number of atomic layers n in the graphene film with n minima indicating $n+1$ graphene layers. While the quantum oscillations are easily identified on free-standing graphene [46], the case of supported graphene is more complicated as the support affects the I(V) curve [45]. Two experiments (shown in Figs. 2 and 3) were conducted with MEM/LEEM as imaging technique which allows for fast data acquisition so that surface changes can be monitored *in-situ*. Applying this microscopy, desorption, and reaction effects are imaged while increasing the sample temperature at a constant rate, as in a temperature programmed desorption (TPD) experiment.

Spatially resolved XPEEM data were recorded at photon energies ranging between 200 and 700 eV. In contrast to MEM/LEEM, XPEEM is a very slow microscopy when acquiring data in the spectral imaging mode. Thus, experiments (shown in Figs. 4–6) using this characterization technique had to be conducted in a way that the graphene sample was cooled to room temperature after having reached a certain state during treatment. However, the spectroscopic characterization can be tuned very surface sensitive, depending on the chosen photon energy. Moreover, choosing a photon energy with an enhanced cross-section, especially for Si 2p at a photon energy of 200 eV pushed the detection limit of the silicon concentration by more than a factor of 10 with respect to a laboratory-based XPS measurement when using Mg K_α or Al K_α radiation. In addition, a novel analysis tool was applied to remove chromatic aberration from image stack data acquired in XPEEM mode [47]. Using this technique, spectral minority phases were imaged at an improved signal-to-noise ratio, which allowed to follow oxygen intercalation and the accompanying segregation of bulk dissolved Si towards the surface below the CVD-grown graphene film.

Fig. 1 displays XPS data acquired using a standard laboratory apparatus containing a hemispherical electron analyzer, a VSW HAC 5000 electronics and a non-monochromatized Al K_α x-ray source.

3. Results and discussion

3.1. Silicon enrichment of the Cu foil by gas-phase transport of released material from the quartz tube reactor

Before addressing the properties of CVD-grown graphene on copper, we demonstrate that the amount of Si impurities at the surface or in the bulk of a Cu foil can be controlled by exposure to hydrogen in a quartz tube reactor at elevated temperatures.

Fig. 1 compiles Si 2p core level data recorded from fresh, bulk-clean Cu foils, which were subjected to two different preparation protocols at
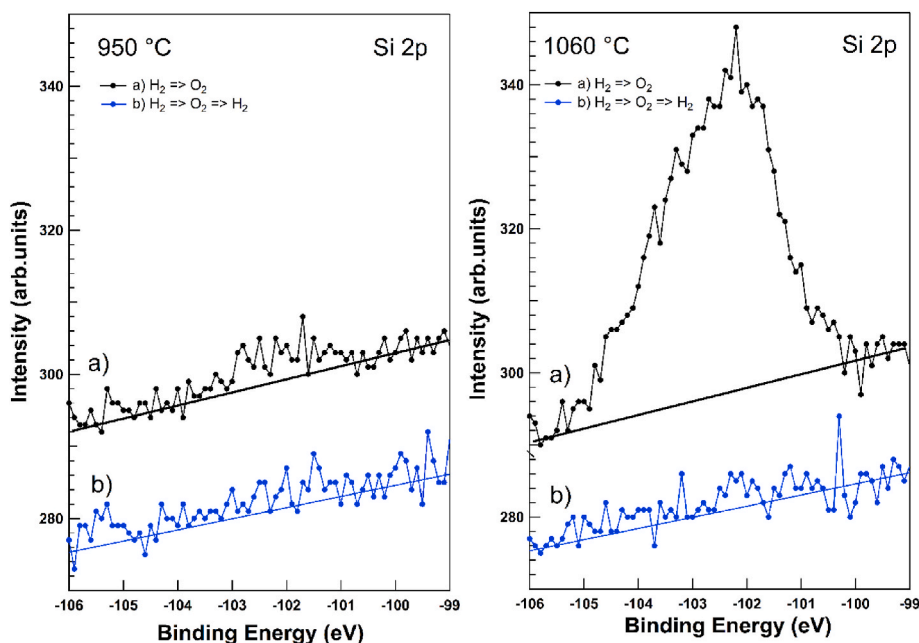

Fig. 1. Cu foil enrichment with Si by H_2 exposure in a quartz tube reactor followed by oxygen-induced Si segregation and its subsequent bulk dissolution during reduction in H_2. a) Cu foil exposure to $p(H_2) = 300$ mbar for 60 min followed by exposure to $p(O_2) = 7.5 \times 10^{-6}$ mbar in 1 mbar Ar for 60 min and subsequent cool down. b) The same exposure sequence as in (a), followed by a final exposure to $p(H_2) = 300$ mbar for 60 min and subsequent cool down. Laboratory-based XPS was used to record the Si 2p data sets in the left and right panels which correspond to equivalent treatments at 950 °C and 1060 °C, respectively. The Si enrichment at the surface in an oxidative environment (top plots) and the reversible Si dissolution upon treatment in hydrogen (bottom plots) can be observed. The effect is barely visible at 950 °C and very pronounced at 1060 °C (see text). (A colour version of this figure can be viewed online.)

950 °C and 1060 °C in our CVD quartz tube reactor. The first protocol a) at 950 °C consists of exposure to 300 mbar hydrogen for 60 min followed by a 60 min treatment in an argon atmosphere of 1 mbar to which an oxygen partial pressure of 7.5×10^{-6} mbar was added and the subsequent cooling to room temperature. Laboratory-based XPS was used for chemical analysis of the treated Cu foils. The Si 2p spectrum taken after gas exposure a) at 950 °C (Fig. 1a - left panel) shows a rather weak and broad Si 2p peak, centered at 102–103 eV, which indicates the formation of SiO_x at the Cu foil surface [48,49] at a concentration just above detection limit of the apparatus. Conversely, when repeating the gas exposure sequence using a fresh Cu foil but adding a second treatment in a hydrogen atmosphere of 300 mbar at 950 °C for 60 min followed by cooling in H_2, the silicon concentration drops below the detection limit (Fig. 1b - left panel). This effect is much more pronounced when performing the preparation at the higher temperature of 1060 °C, as seen in the right panel of Fig. 1. Here, an equivalent H_2 treatment followed by Ar + O_2 exposure was carried out, producing the pronounced accumulation of Si, as evidenced by the large photoelectron emission from the Si 2p core level. Again, a broad peak between 102 and 104 eV indicates the formation of silica on Cu, without reaching the oxidation state of bulk SiO_2 [48,49]. When repeating the treatment on a fresh Cu foil and conducting the additional exposure to hydrogen (p(H_2) = 300 mbar for 60 min) before cooling the sample in the reductive atmosphere, no silicon was detected on the Cu foil surface.

The used Cu foils were proven to be Si-free initially because the described oxygen-induced Si enrichment in the Ar + O_2 atmosphere was not observed when omitting the high pressure H_2 treatment before exposure to oxygen (not shown). We conclude that the accumulating silicon on the Cu foil is released from the reactor wall and transported through the gas phase. The process was shown to be mostly influenced by the aging of the used quartz glass and the duration of the hydrogen exposure at T > 950 °C. The release of Si from the reactor wall and the related gas-phase transport have already been addressed in the literature. It is likely that the most abundant species is gaseous SiO, which was found to be the main reaction product of fused silica in contact with hydrogen at elevated temperatures [41]. We suggest that hydrogen exposure at 300 mbar induces the release of SiO from the reactor wall which adsorbs on the Cu surface where it is rapidly reduced by hydrogen and dissolves in the bulk. As a result, the surface concentration of Si drops below the detection limit of a typical laboratory-based XPS system. However, if a Si-loaded Cu foil is exposed to oxygen, Si segregates at the Cu surface where it forms silica. The data compiled in Fig. 1 demonstrate that the surface accumulation of silica and dissolution of reduced silicon are, to a large extent, reversible processes.

Since graphene CVD growth is typically performed at temperatures above 1000 °C in a hydrogen-rich atmosphere, the Cu foil can be readily loaded with Si transported through the gas phase already during graphene growth. However, as long as the Si oxide layer is reduced by hydrogen, Si atoms can easily dissolve in the bulk of the Cu foil. As Si does not accumulate on the surface during CVD growth, we can infer that it does not influence the graphene growth significantly. However, graphene grown on Si-loaded or Si-free Cu foils will behave differently after removal from the CVD reactor. In the following, we will examine the uptake of adsorbates and intercalants during exposure to air, their fate during annealing in vacuum and their effect on the morphology and chemical state of the graphene film and interface. It will be shown that exposure to air or to oxygen in presence or absence of dissolved Si in the Cu foil influences the properties of the grown graphene layer, especially affecting its resistivity towards oxidation.

### 3.2. Intercalation/de-intercalation below CVD-grown graphene on silicon-free Cu foils

In this subsection, we discuss the properties of graphene grown on Cu foils that were not exposed to large amounts of silicon prior to or during CVD synthesis after their exposure to air. Fig. 2 displays the edge of a CVD-grown graphene flake on Cu which has been exposed to air for two weeks after CVD synthesis. The sample was introduced in the spectroscopic photoemission and low energy electron microscope (SPELEEM) "as is" without annealing of the sample for degassing purposes. At first, the graphene layer was characterized by micro-spot low energy electron diffraction (μ-LEED), limiting the electron beam illumination to a 5 μm wide area. No diffraction pattern could be observed at the beginning, but prolonged irradiation with 85 eV electrons resulted in the slowly appearing faint hexagonal LEED pattern of the graphene lattice, indicating the removal of a disordered surface layer on graphene. This is consistent with stimulated dissociation and desorption processes occurring upon irradiation with electrons at energies above 15 eV.

Having observed that graphene on Cu after long exposure to air is sensitive to electron illumination, subsequent characterization should minimize irradiation-induced changes to the surface. Therefore, the sample was imaged with minimum electron kinetic energy at a start voltage (STV) of 0.25 V in the mirror electron microscopy (MEM) mode (also see experimental section). Fig. 2a displays MEM images of a CVD-grown graphene flake (image top) and the partially-exposed Cu foil surface (bottom) taken during a temperature programmed desorption (TPD)-type experiment. The field of view (FOV) is 40 μm. Three wrinkles in the graphene layer appear as parallel lines propagating diagonally from the upper left to the right bottom. The dark rim on the bare Cu surrounding the flake stems from the electron irradiation during microscope alignment prior to the measurement. At this point, electron irradiation has already permanently modified the sample. The effect of electron illumination at high kinetic energy is also seen by the dark ring-shaped structure on the graphene flake enclosing the micro-spot of the previously performed μ-LEED measurement with 85 eV electrons.

The MEM images of Fig. 2a display snapshots of the g/Cu sample at selected temperatures while annealing from 50 to 380 °C at a rate of 0.5 K/s. A movie of the recorded images during temperature ramping is found in the Supplementary information together with the background pressure recording of the microscope chamber. During temperature ramping, the pressure raised exponentially up to 80 °C followed by a slower exponential increase up to 180 °C where it levelled off at $(1.3–1.8) \times 10^{-6}$ mbar. After exceeding 350 °C, the background pressure dropped until reaching the final temperature of 380 °C of the movie. From then on, the temperature ramp was continued up to a final temperature of 450 °C at reduced rate of 0.16 K/s while the background pressure continuously dropped further. As shown in the Supplementary information, the significant pressure increase during sample annealing indicates substantial desorption from the sample and sample holder which can be quantified by integrating the background pressure to give a sum value of 620 Langmuir (L) of the performed annealing experiment.

The movie sequence and the displayed MEM images of Fig. 2a provide contrast which reflects temperature-induced desorption processes on the g/Cu sample. During temperature increase up to ~120 °C, the electron reflectivity (measured at the start voltage of 0.25 V) decreases leading to the darker appearance of the entire graphene flake, which can be attributed to a decrease of the local work function. Small, faint hexagonal patches appear in graphene which can be identified as bilayer graphene (BLG) islands (see below). The overall intensity decrease observed in MEM can be attributed to the desorption of a disordered adsorbate layer covering graphene in agreement with the observed background pressure increase. In the temperature range between ~200 and 270 °C, fronts in the graphene layer are observed, propagating *inwards* from the flake edge and the wrinkles (see blue arrows). The dark patches on the flake are surrounded by these fronts, their size decreasing with increasing temperature. Since front-type contrast changes are incompatible with simple adsorbate desorption which should occur on every part of the surface with equal probability, the contrast must stem from the desorption of an intercalant which agrees to the increasing background pressure (reaching the 10^{-6} mbar range). Thus, we attribute this contrast to the removal of an intercalated species I_a, which diffuses under graphene and desorbs when reaching either the flake edge or a
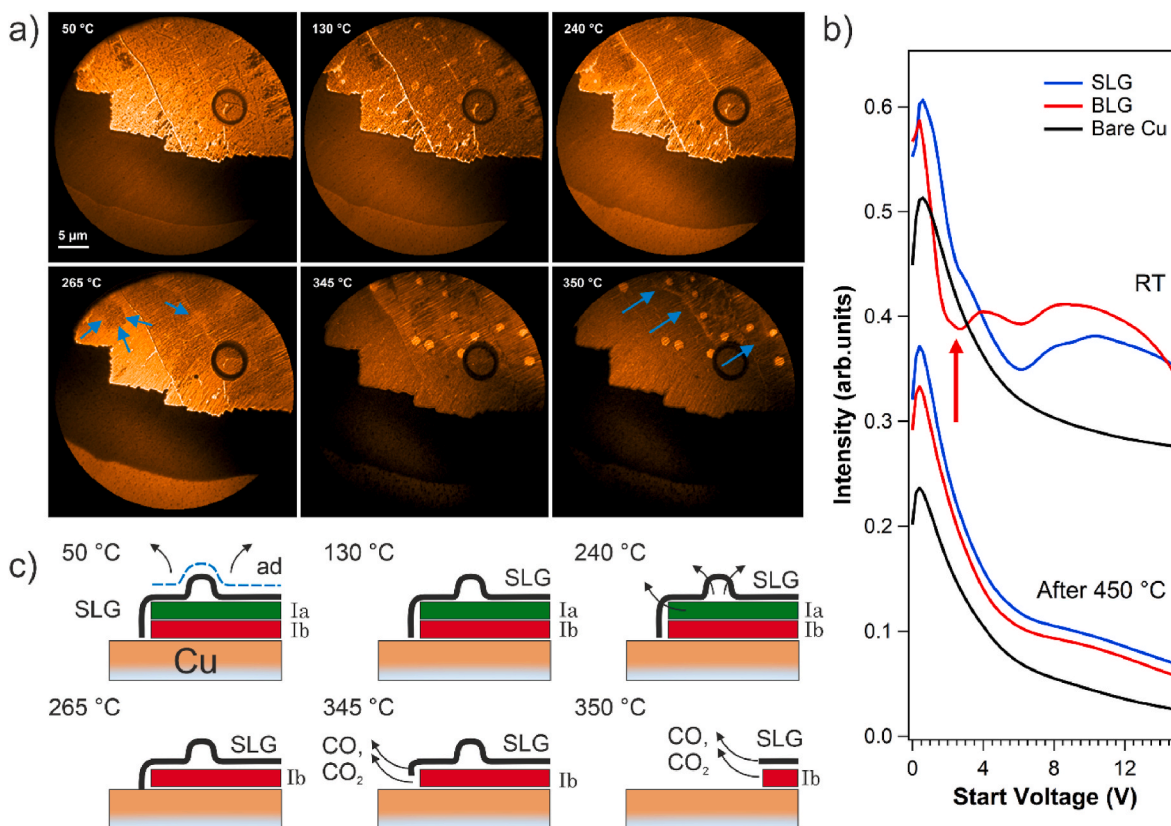
Fig. 2. a) MEM images (STV = 0.25 V, FOV = 40 μm) acquired during the first annealing of a pristine graphene on Cu (g/Cu) sample after exposure to air for two weeks in a temperature programmed desorption (TPD) experiment. b) LEEM I(V) curve taken before and after the TPD experiment. A red arrow indicates the minimum in the electron reflectivity curve taken from the small hexagonal islands inside the graphene flake. The minimum stems from quantum oscillations and identifies the small hexagonal islands as BLG inside the SGL flake. The absence of any oscillations in the LEEM I(V) curve after annealing to 450 °C indicates the removal of the CVD-grown graphene. The contrast-enhanced MEM images at 345 °C and 350 °C demonstrate the onset of the SLG removal, increasing the contrast of the remaining BLG islands, which were removed above 420 °C (see text). (Movie available as Supplementary information). c) Sketched sequence of the observed adsorbate and intercalate removal. (A colour version of this figure can be viewed online.)
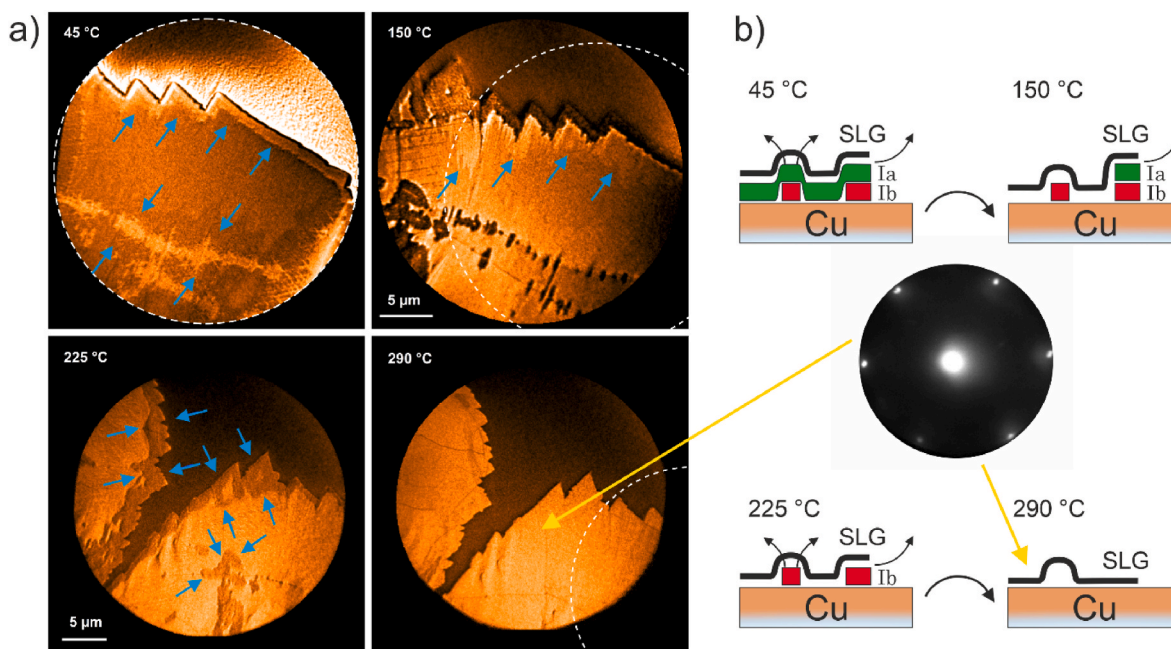
Fig. 3. a) MEM image sequence (STV = 0.75–1.15 V, FOV = 30 μm) acquired during the stepwise annealing to 290 °C of a g/Cu sample after exposure to air for 3 days. b) Sketches of the intercalate removal. Inset: The hexagonal diffraction pattern of graphene taken at 60 eV after the sample annealing indicates that the intercalate removal did not attack the graphene layer. (Movies available as Supplementary information). (A colour version of this figure can be viewed online.)
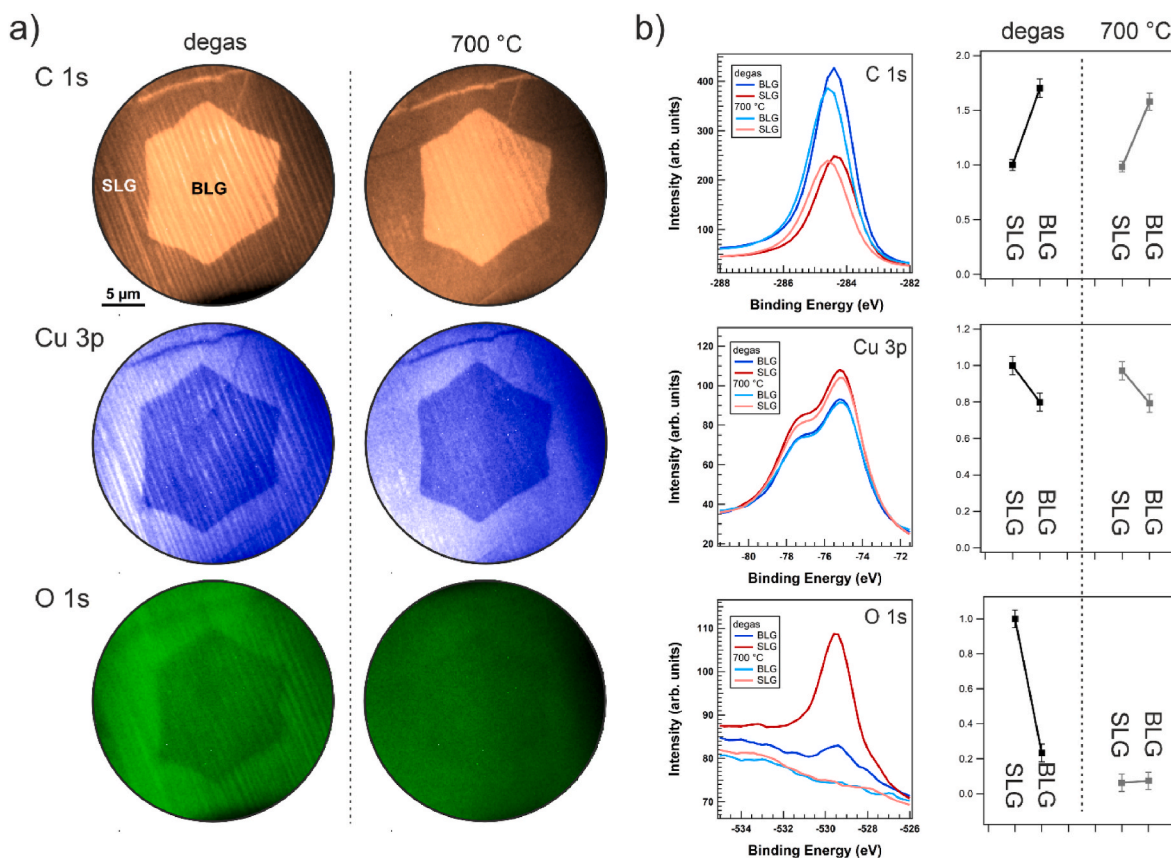
Fig. 4. XPEEM data of a Cu foil entirely covered by CVD-grown graphene after 1 week of exposure to air. The data were acquired at room temperature after vacuum degas at 200 °C for 2 h and after annealing to 700 °C. a) C 1s, Cu 3p and O 1s image (FOV = 30 μm, hν = 640 eV, total x-ray irradiation time 1.5 h) b) Area selective C 1s, Cu 3p and O 1s spectra from SLG and BLG (left column) together with the integrated peak intensities before and after annealing (right column). The data prove that oxygen intercalated between graphene and the Cu foil and was entirely removed during annealing to 700 °C without affecting the covering graphene layer (see text). (A colour version of this figure can be viewed online.)

wrinkle. At temperatures above ~320 °C, the electron reflectivity drops drastically. Applying a 2-times enhanced greyscale in the displayed MEM images resolves a second front which propagates from the edge towards the inner part of the graphene flake. Blue arrows point to this front in the MEM image acquired at 350 °C. Note that the areas originally covered by BLG islands appear with high intensity at 350 °C. The contrast vanishes almost completely when exceeding 420 °C (not shown). As will be discussed in the following, we attribute this second front to the complete removal of the SLG film. Before and after having finished the TPD experiment in MEM imaging (Fig. 2a), real space LEEM images were acquired as a function of the start voltage (see Experimental section). Extracting the intensity of the bare Cu foil, the small hexagonal islands and the surrounding graphene flake from the acquired LEEM I(V) data set leads to the curves, which are labeled bare Cu, BLG and SLG in the plot shown in Fig. 2b. Before annealing, they show quantum oscillations in the electron reflectivity between 0 and 5 eV. A red arrow points to the minimum characteristic for bilayer graphene, identifying the small hexagonal islands as BLG nucleated in the SLG flake [45,46]. The electron reflectivity of the bare Cu area surrounding the flake displays no intensity modulations, which will be discussed below. After annealing to 450 °C and cooling down, no electron reflectivity oscillations were observed anymore on the entire sample. Thus, we conclude that the graphene was removed from the surface during the annealing experiment and propose that the onset of SLG removal is resolved by MEM imaging above 345 °C. Note that the SLG removal increased the contrast of the small hexagonal BLG islands in Fig. 2a. However, the contrast of the BLG islands was not observed above 420 °C anymore (not shown in Fig. 2) in agreement with the almost identical I(V) curves

acquired from the former SLG and BLG regions after the TPD experiment which indicates the complete removal of the entire graphene film.

As sketched in Fig. 2c, we postulate the presence of an oxygen-containing species I_b intercalated underneath the graphene layer, which remained on the sample at 265 °C after the desorption of species I_a and completely burned off the graphene flake from the Cu support at 345 °C and above. Of course, species I_a and I_b do not necessarily have to be stacked on top of each other as sketched in Fig. 2c but may coexist in laterally separated phases. However, species I_b remains immobilized at temperatures where species I_a already diffuses underneath graphene and desorbs from the g/Cu sample.

It should be noted that the featureless energy-dependent electron reflectivity of the (0,0) beam observed on the bare Cu foil is not expected at first glance. Prior to CVD synthesis, reaction steps are performed that turn the poly-crystalline Cu foil into faceted Cu(100) surfaces [50] or (following a more recent pre-treatment) into faceted Cu(111) surfaces [13,15,16,46] which should exhibit pronounced intensity modulations of the LEEM I(V) curve. However, prolonged exposure to air induces the formation of an amorphous Cu oxide layer which turns the Cu support surface non-crystalline explaining the almost featureless electron reflectivity curve extracted from these areas.

We can now discuss the formation of a ring-shaped region around the illumination spot of the μ-LEED experiment. LEEM I(V) curves extracted from the dark ring area of the MEM image in Fig. 2 are identical to the ones extracted from the bare Cu surface, which proves the complete graphene removal along the perimeter of the electron-irradiated region. Interestingly, the electron-irradiated area itself slowly developed the LEED pattern of graphene with time. This suggests that the electron

beam has induced the formation of a mobile species which diffused out of the irradiation zone and reacted off the covering graphene layer along its rim.

Summarizing the observations of the annealing experiment in Fig. 2, the MEM data indicated the existence of an adsorbate on top of the graphene flake and two different processes relating to intercalants underneath graphene on a sample which was in contact with air for two weeks. The first one led to a mobile species which desorbed between 200 °C and 270 °C when ramping up the temperature at 0.5 K/s while the second one caused the removal of the graphene layer at temperatures above 320 °C. While it is most probable that each involved intercalated species contains oxygen, the intercalate of the second process must contain oxygen since graphene can only be removed during vacuum annealing by oxidation. The observed oxidation of the graphene flake at temperatures above 320 °C fits well with the temperature reported in an *in-situ* study where oxygen exposure above 360 °C leads to intercalation and etching of the covering graphene layer [51]. Note that burning off an entire layer of SLG with a surface coverage of more than 2 monolayers (ML) on low-indexed Cu surfaces requires a substantial amount of oxygen.

In order to prove that the concentration of the intercalated oxygen at temperatures above 320 °C plays a crucial role, the temperature programmed desorption experiment was repeated. But now, a freshly synthesized g/Cu sample exposed to air for only three days before characterization by LEEM was used and the annealing in ultra-high vacuum (UHV) was performed stepwise. The first temperature ramp was conducted again at the rate of 0.5 K/s but stopped after reaching ~220 °C, keeping this intermediate temperature constant for about 80 min. The subsequent temperature increase up to 290 °C was performed at the much lower rate of 0.04 K/s and the sample was kept at the final temperature for 30 min before ending the data acquisition.

Fig. 3a displays MEM images (STV between 0.75 V and 1.15 V) taken during the stepwise annealing of the sample in UHV. (Two movies are available as Supplementary information.) Note that during data acquisition, the sample moved laterally due to thermal expansion of the sample mount. The dashed circle shown in the image at 150 °C and 290 °C indicates the position of the first image in the data set. Similar to the data shown in Fig. 2, the background pressure during annealing raised significantly, although it remained below 5×10^{-7} mbar during the experiment. During the two temperature ramps of Fig. 3a, the background pressure accumulated a value about 3-times smaller than the 620 L derived in the experiment of Fig. 2. We thus conclude that the g/Cu sample with 3 days of contact to air released less material during annealing with respect to the one with an exposure time of 2 weeks (see Supplementary information). In addition, and possibly more important, the stepwise annealing sequence led to an about two orders of magnitude lower pressure increase at temperatures above 220 °C. The MEM images of Fig. 3a display the edge of a graphene flake (bottom) together with the neighboring bare Cu surface (top) in the field of view (FOV) of 30 μm. Notably, during annealing up to ~100 °C, the MEM intensity did not change. Upon further annealing to ~150 °C, a reaction front-type propagation was observed, moving along the wrinkles and close to the flake edge (see arrows).

Similar to the case in Fig. 2, we attribute the observed contrast change in MEM to the presence of an intercalated species I_a under the graphene layer, which escapes at wrinkles and along the flake edge as sketched in Fig. 3b. When reaching a temperature of 225 °C, dark patches in the graphene flake along its perimeter and along wrinkles are observed, marked by blue arrows in the figure. This observation proves that, again, a second intercalated species I_b remained underneath the graphene flake, as also sketched in Fig. 3b. However, now the species I_b remained at small portions of the surface close to the flake edge or close
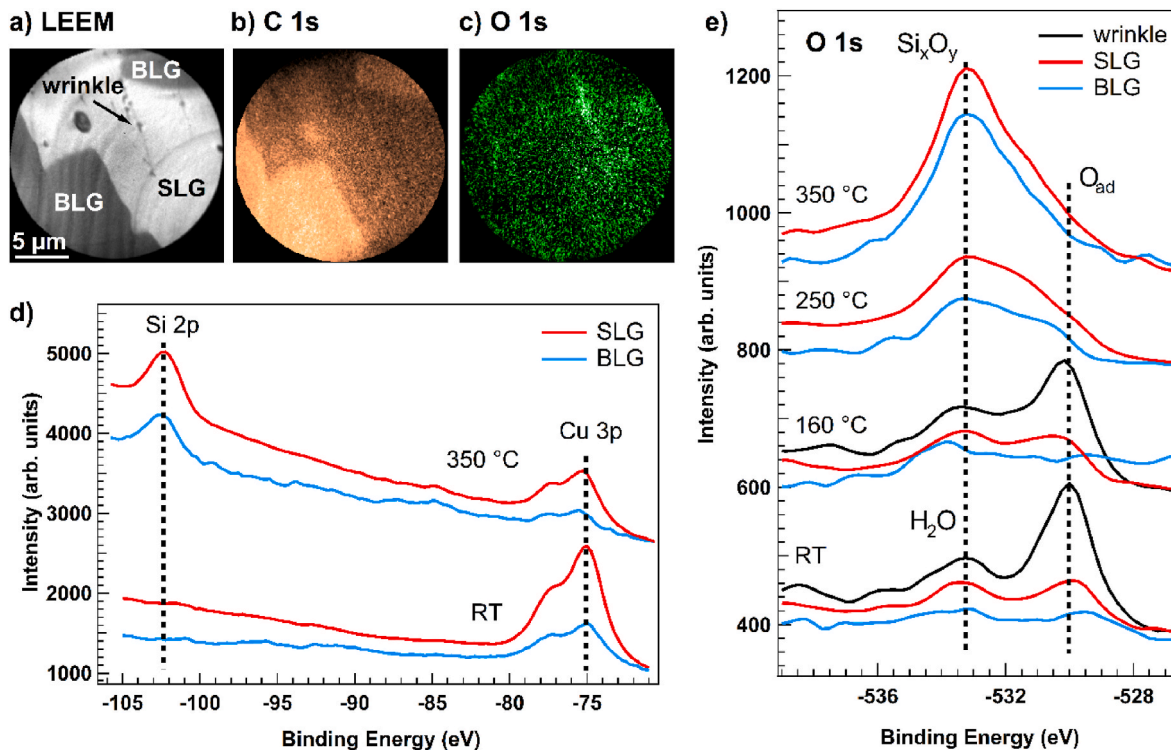

Fig. 5. LEEM/XPEEM data acquired from synthesized graphene on a Cu foil which contained dissolved Si in the bulk after two weeks of exposure to air. Images with FOV = 20 μm of the pristine sample before annealing: a) LEEM image at STV = 1.6 V b) C 1s and c) O 1s image taken at a photon energy of 700 eV. d) Si 2p and Cu 3p of the SLG and BLG region taken at a photon energy of 200 eV show no Si 2p emission before annealing to 350 °C and a substantial Si 2p peak afterwards. e) Area-selective O 1s spectra taken at room temperature (RT) and after annealing to 160 °C, 250 °C and 350 °C using 700 eV photons (total x-ray irradiation time 12 h). The conversion of the O 1s species at ~530 eV towards a species at 533.5 eV is well resolved (see text). All displayed data were acquired at room temperature. (A colour version of this figure can be viewed online.)
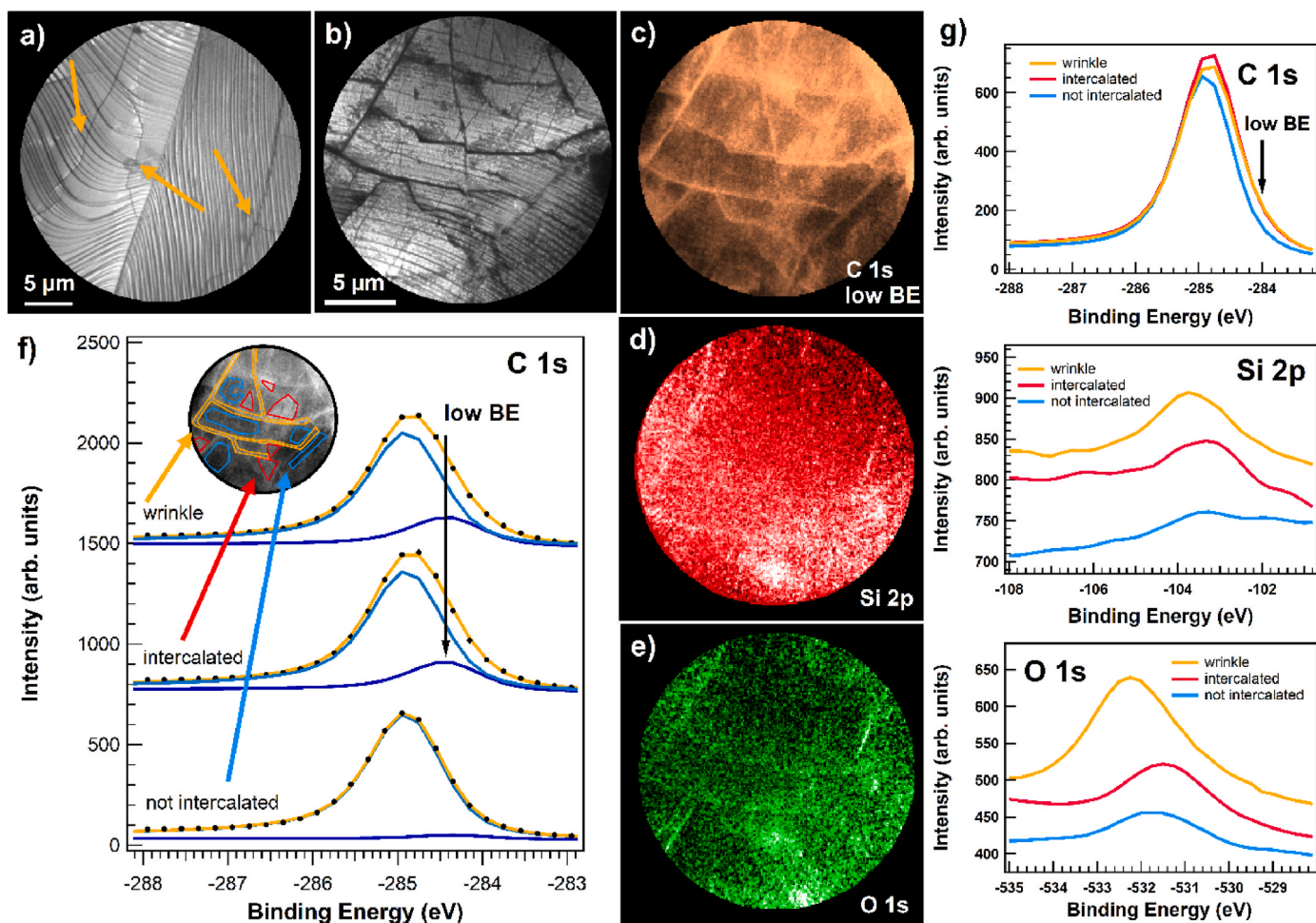
Fig. 6. LEEM/XPEEM data of a CVD-grown graphene film on a Cu foil with dissolved Si in the bulk which has been exposed to air for 2 weeks. a) LEEM image of the pristine sample taken after 17 h degas at 80 °C and cool down to room temperature (STV = 2.0 V, FOV = 30 μm). Subsequently, the sample was exposed to 600 L O$_2$ at p(O$_2$) = of 1×10^{-6} mbar and temperatures between 650 and 700 °C and finally cooled down to room temperature for further characterization: b) LEEM (STV = 20 V, FOV = 20 μm), c) C 1s low binding energy image, d) Si 2p image, e) O 1s image, f) area-selective C 1s spectra, g) area-selective C 1s, Si 2p and O 1s spectra. The C 1s and Si 2p data were acquired at a photon energy of 400 eV, and the O 1s data by using 650 eV photons (total x-ray irradiation time 2 h). (A colour version of this figure can be viewed online.)

to wrinkles. The removal of this species by traveling fronts is well resolved by MEM and completed when reaching 290 °C. The front motion towards the wrinkles and the flake edge indicates the desorption of the intercalant I_b where it can reach the gas-phase boundary of the sample, as sketched in Fig. 3. In contrast to the experiment in Fig. 2, the graphene flake remained stable at 290 °C, demonstrated by the observation of a sharp hexagonal diffraction pattern ascribed to SLG (see inset). Thus, we conclude that at this stage, no further intercalant was present anymore which could react with the graphene layer.

Comparison of both data sets helps to identify the two intermediate species I_a and I_b. I_a must be a species that rapidly intercalates during air exposure as it appears on both samples. The most likely species are gaseous oxygen or water. Both adsorbates are expected to readily diffuse underneath graphene and desorb during annealing in vacuum when overcoming their thermal activation barrier. The I_b species, instead, is observed only at areas in close vicinity to wrinkles and along graphene flake edges and accumulates to a great extent only after long-time exposure to air. We suggest that I_b can be attributed to Cu oxide. This stems from the fact that the formation of Cu oxide requires long-time exposure at high oxygen partial pressure due to its slow formation kinetics. Consistent with this interpretation, I_a already de-intercalates at low temperatures while the de-intercalation of I_b requires the decomposition of Cu oxide via the reaction of CuO to Cu$_2$O at T > 200 °C and

the reduction of the latter towards metallic Cu at T > 400 °C [52]. The oxygen adatoms released following oxide decomposition then desorb from Cu when being in close vicinity of a wrinkle or a flake edge. If this geometry is not met or if the oxygen release rate exceeds its desorption rate, the freely diffusing oxygen accumulates and erodes the graphene at its edges, reacting off the entire flake. The assignments of I_a and I_b are in accordance with the given interpretation of the MEM data sets shown in Figs. 2 and 3. On the sample only briefly exposed to air, the I_b intercalant was found exclusively in areas where direct gas-phase contact could occur and where the oxide decomposition front at T > 220 °C was observed. Instead, long-time air exposure led to Cu oxide formation below graphene over much wider areas (Fig. 2), so that the thermally induced oxide decomposition produced sufficient oxygen to burn the entire graphene flake off the surface.

Complete removal of the intercalant from the graphene sample with short contact time to air was observed after annealing above 290 °C. This is proven by the fact that, at this stage, graphene did not show any beam-induced effects, even when using electron energies above 100 eV and irradiating for a long time. This finding also supports the attribution of I_b to Cu oxide, as its beam sensitivity is known to result from the exposure to low energy secondary electrons [53], so that extensive irradiation would deteriorate the oxide and, consequently, the graphene layer. Instead, the graphene removal from the ring area surrounding the

irradiated zone observed in Fig. 2 possibly originates from a different, much faster process. We suggest the presence of intercalated water under the graphene layer. Irradiation of this species would lead to the known formation of gaseous radicals which diffuse outside of the irradiated zone and attack the graphene layer [54,55].

Finally, we discuss the possible presence of an adsorbate layer on top of graphene. The absence of such a layer on top of graphene after 3 days of exposure to air underlines the low reactivity of graphene. However, after air exposure for 2 weeks, such a layer builds up as evidenced by the data compiled in Fig. 2. While the exact nature of such an adsorbate layer on top of graphene remains speculative, it can be stated that the layer is removed already during a mild vacuum annealing at 100 °C. Potential candidates for such an adsorbate layer are hydrocarbons or carbonates, maybe in combination with adsorbed or intercalated water, especially slowly accumulating at defects in the graphene layer.

In the following, we present XPEEM spectroscopic data that support the qualitative picture derived from the already discussed LEEM data. Since XPEEM data acquisition is much slower, *in-situ* TPD experiments cannot be performed. Instead, sample characterization was accomplished after annealing to a certain temperature and cooling down. Fig. 4 displays images and spectra from a Cu foil, entirely covered by CVD-grown graphene, taken at room temperature after annealing at 200 °C and 700 °C in UHV. The sample was exposed to air for 1 week before the XPEEM analysis. The acquisition of the XPEEM data sets shown in Fig. 4 required x-ray irradiation for 1.5 h. In order to reduce potential beam damage, the sample was pre-annealed in vacuum to 200 °C and all adsorbates were desorbed. Thus, only intercalated species I_a and I_b may be present, trapped underneath graphene.

Fig. 4 compiles C 1s, Cu 3p and O 1s photoelectron XPEEM data of the sample acquired upon irradiation with 640 eV photons which supports these expectations. In the image center, a 10 μm wide bilayer graphene region is visible, appearing bright in the C 1s image and dark in the Cu 3p and O 1s images of Fig. 4a. The XPEEM data consist of a stack of energy-filtered photoelectron images acquired at increasing photoelectron kinetic energy. Extracting the intensity from the SLG and BLG region of the imaged field of view at the given photoelectron energy allows to plot spatially resolved C 1s, Cu 3p and O 1s core level spectra. The spectra, taken before and after annealing to 700 °C, are plotted in Fig. 4b together with the integrated peak intensities which are scaled to the corresponding intensities recorded from SLG before annealing.

The C 1s image maps the photoelectron emission intensity at the peak maximum and displays the BLG island almost twice as bright as the surrounding SLG. Such a difference is observed if the released photoelectrons are only weakly attenuated by the additional layer in BLG. Namely, the BLG C 1s signal appears just 1.7-times brighter than that of SLG indicating that the additional layer in BLG still provides about 70 % of the intensity of SLG. Such a modest signal attenuation is consistent with the 355 eV kinetic energy of the released C 1s photoelectrons [54, 56]. Opposite to C 1s, the Cu 3p images exhibit an inversion of contrast, as the emitted Cu 3p photoelectrons are damped by the top graphene layers. Here, the signal damping is less severe due to the higher kinetic energy of the released photoelectrons (565 eV) so that the Cu 3p intensity is attenuated by only 20 % per additional graphene layer.

Finally, we note that the O 1s images show a larger contrast before sample annealing to 700 °C. In fact, the O 1s spectrum from the SLG region has a more than 4-times larger intensity than the one obtained from the BLG island. The observed signal attenuation under BLG is slightly larger than the expected value (3-times) obtained when considering the 110 eV kinetic energy of the released O 1s photoelectrons [56]. The deviation of both numbers slightly exceeds the error bar of the experiment and might indicate that oxygen intercalation below BLG is kinetically hindered.

After annealing to 700 °C, the O 1s spectra show no detectable signal. Correspondingly, the O 1s map does not provide any chemical contrast despite the almost vanishing background level change in the BLG region, suggesting that all oxygen has been desorbed. On the other hand, the C

1s map is very similar to that obtained before annealing. This proves that the CVD-grown SLG and BLG are the outermost layers, i.e., the oxygen signal must have been emitted by an intercalated species located at the graphene-Cu interface. Further evidence supporting that oxygen was intercalated beneath graphene comes from the observed C 1s shift towards high binding energy observed after annealing. This agrees well with literature data reporting that the n-doping of CVD-grown graphene on metallic Cu decreases upon oxygen intercalation between graphene and Cu [24]. We note that the Cu 3p photoelectron emission yield from under SLG and BLG is essentially unaffected after annealing to 700 °C. This allows us to conclude that the amount of intercalated oxygen must be well below one monolayer, i.e., the intercalant must have been adsorbed oxygen and not a thick oxide. Note that the formation and decomposition of Cu oxide would have induced a much larger effect on the Cu 3p signal intensity because the Cu packing density between Cu oxide and metallic Cu differs substantially. The Cu 3p peak position remained at constant energy upon annealing to high temperature, and the observed O 1s peak position of about 530 eV is compatible with the identification of O_{ad} on Cu (O 1s binding energy of 530.0 eV on Cu(110) at low and 530.7 eV at high coverage of O_{ad}) [57]. We point out that the observed broad O 1s peak energy does not allow us to rule out the presence of oxygen in an oxidic environment as these species exhibit very similar O 1s binding energies (O 1s binding energy of 530.4 eV in Cu_2O and 529.6 eV in CuO) [58]. However, the observed O 1s intensity can be compared to the one obtained from a recently reported 2-dimensional silica phase on Cu(111) [59], indicating a sub-monolayer coverage of intercalated oxygen, also ruling out the assignment to Cu oxide (see the Supplementary information). The XPEEM experiment of Fig. 4 was conducted using a SLG film entirely covering the Cu support. This fact might explain why intercalated oxygen is still found after degassing at 200 °C, while it was removed from graphene flake samples already at this temperature (see Figs. 2 and 3). We also cannot rule out that potential Cu sub-oxide decomposed during degassing at 200 °C and not all released oxygen de-intercalated but got trapped under the covering graphene film. However, the trapped oxygen amounted to a small quantity so that it was removed from the interface during annealing to 700 °C without attacking the covering graphene layer. Similar to the case shown in Fig. 3, after having removed all intercalants, the supported graphene layer can be heated to any temperature in vacuum without degradation and does not show any beam sensitivity.

Oxygen exposure at high temperatures under UHV conditions does not affect such g/Cu samples for a long time due to the low sticking of oxygen on the inert surface. However, if a substantial amount of oxygen makes it to the surface, the graphene is immediately burned and removed from the Cu surface [24,51]. This behavior changes when dealing with Si-enriched Cu foils.

3.3. Intercalation/de-intercalation below CVD-grown graphene on silicon-enriched Cu foils

Fig. 1 already proved that Cu foils can be loaded with Si through gas-phase transport of released material from the quartz reactor wall. Si-enrichment of the support foil may occur in the reductive atmosphere during graphene CVD synthesis, or it can be forced on purpose by annealing in pure hydrogen prior to CVD growth at p > 100 mbar and T > 1000 °C. If the sample treatment including sample cooling is performed in an oxygen-free gas atmosphere, the Cu foil remains Si-loaded but, as Si is highly diluted, the Si surface concentration remains well below XPS detection limit.

Fig. 5 displays LEEM/XPEEM data taken from such a Si-pre-loaded Cu foil entirely covered by CVD-grown graphene. The sample was kept in air for 2 weeks prior to analysis. The pristine sample was introduced in the XPEEM chamber and characterized before and after subsequent annealing steps in vacuum. Fig. 5a displays a LEEM image at STV = 1.6 V. While areas covered by SLG appear bright, two BLG islands at the lower left and upper right corners are imaged dark. A prominent

wrinkle is resolved as a dark vertical line in the SLG region. The dark elliptical spot represents a region where μ-spot electron irradiation was carried out prior to the LEEM/XPEEM analysis, altering the sample surface. This region was excluded from the analysis. Fig. 5b shows the C 1s image of the same area, clearly identifying the enhanced C 1 s intensity in the BLG regions, at the electron beam irradiated spot and along the folded wrinkle. The O 1s image in Fig. 5c suffers from low statistics but provides high contrast along the vertical wrinkle. The slightly lower O 1s intensity in the BLG regions is even less visible due to the low signal-to-noise of the data. Similar to the data shown in Fig. 4, we can define three regions of interest: "SLG", "BLG" and "wrinkle" from which local Si 2p + Cu 3p and O 1s spectra were extracted and compiled in the panels of Fig. 5d and e, respectively.

As expected, the pristine Si pre-loaded Cu foil does not display any Si at its surface, which is evidenced in Fig. 5d by the local SLG and BLG XP spectra spanning the energy range of the Si 2p and Cu 3p core levels. The absence of any Si 2p emission proves a silicon concentration below 0.006 ML, which is the approximate detection limit for Si 2p at the chosen photon energy of 200 eV (see Supplementary information). This also holds for the spectra taken along the wrinkled region which are identical to the ones taken from SLG (not shown). The observed signal loss of the Cu 3p emission from BLG with respect to the one from the SLG region by about 70 % fits the photoelectron damping of a full graphene layer at the kinetic energy of 125 eV [56]. The O 1s spectra acquired from the pristine sample contain a pronounced peak at ~ 530 eV which can be attributed to intercalated oxygen in an adsorbed or oxidic environment. The O 1s intensity of this species can be compared to the oxygen loading of the reference 2-dimensional silica phase on Cu(111) [59] indicating a sub-monolayer oxygen coverage below the covering graphene which would identify the intercalated oxygen species as O_{ad} (see Supplementary information). Interestingly, a second O 1s peak with a binding energy of about 533 eV is also observed which cannot be attributed to Cu oxide [52] but rather indicates the presence of water on the non-annealed g/Cu sample [54].

After data acquisition at room temperature, the sample was stepwise annealed to 160 °C, 250 °C and 350 °C and, after each step, cooled to room temperature and characterized by XPEEM. The C 1s peak intensity of the SLG and BLG region did not decrease during the entire experiment of Fig. 5 so that the covering graphene layer must have remained intact after each annealing step. Thus, each surface species characterized by the compiled spectra in Fig. 5d and e are intercalated species below the covering graphene layer. The O 1s spectra clearly indicate that the 530 eV O_{ad} species remains on the surface until 160 °C but vanishes at higher temperatures. However, this oxygen is not removed from the surface but rather converted into another oxygen species exhibiting an O 1s binding energy of 533 eV, which gradually grows at the cost of O_{ad}. The oxygen intercalant is also laterally redistributed. While the oxygen accumulation along the wrinkle is still seen after annealing to 160 °C, the contrast in the O 1s image vanishes upon annealing at 250 °C. Since the 530 eV O 1s species vanishes almost completely, the intercalated O_{ad} must have become mobile enough to laterally diffuse below graphene and convert into the new 533 eV species. As a result, above 250 °C, the O 1s spectra taken from the plain SLG and the wrinkle area are identical and only the spectrum of SLG is shown, now indicating the almost complete absence of the O 1s peak at 530 eV and pronounced photoemission at 533 eV. At T ≥ 250 °C, water should already be desorbed and, in fact, the attribution of the 533 eV O 1s species to water can be ruled out, since intercalated water can only diminish during vacuum annealing while the 533 eV O 1s intensity increases with increasing temperature. The XPEEM data of the Si 2p + Cu 3p spectral region (Fig. 5d) resolve the issue of finding a correct O 1s assignment as they prove the appearance of a Si 2p peak, i.e., an increase of the Si surface concentration. The observed Si 2p peak energy of about 103 eV indicates the formation of a surface silica phase which agrees with the observation of an O 1s peak at a binding energy of about 533 eV at T ≥ 250 °C since it ranges between the values reported for surface silica on Cu(111) [48] and SiO_2 [49]. In

the Supplementary information, the O 1s peak intensity and the Si 2p to Cu 3p peak intensity ratio of the data acquired after annealing to 350 °C are compared to the numbers extracted from the reference 2-dim silica phase on Cu(111), indicating an oxygen loading lower than, and a Si concentration similar to the one of the reference structure. Note that the acquisition of the spectral data required x-ray irradiation for about 12 h which explains why the signal-to-noise ratio of the acquired data could not be further improved any further.

Summarizing the above observations, we conclude that high vacuum annealing of CVD-grown g/Cu in presence of bulk dissolved Si does not induce de-intercalation of intercalated oxygen, but rather triggers its conversion into intercalated silica which requires Si segregation and accumulation at the Cu surface. Since the latter needs surface mobility of Si atoms, the formation of silica can only take place at elevated temperatures. Thus, if the removal of adsorbates and intercalated oxygen is desired, the sample must be degassed well below 160 °C, e.g., at 120 °C. In this case, no Si enrichment on the Cu foil is expected. If, however, the annealing temperature exceeds 250 °C, Si segregation will take place when oxygen-containing species are present intercalated under graphene.

Using Cu foils with bulk dissolved Si for graphene synthesis offers the possibility of decoupling graphene from the Cu support without further need to intercalate Si and oxygen in separate preparation steps as was done by Larciprete et al. [60] but can be achieved in a simple step following CVD synthesis. Moreover, the Si segregation process can be initiated in the CVD reactor itself and might even take place during synthesis if the reactive atmosphere is contaminated by a minority oxygen partial pressure during or after synthesis. Due to the low Si concentration involved and due to the rather low sensitivity of laboratory-based XPS towards Si (see Supplementary information) these effects could not be observed in earlier studies.

At variance to the case of Si-free Cu foils, where the oxygen intercalant is either removed or burns off the graphene layer, the Si atoms act as oxygen scavengers as they strongly bind the intercalated oxygen in a surface silica phase. As a result, CVD graphene seems to be oxygen resistant, i.e., it is tolerant to oxygen present in the reactive gas atmosphere. This fact has been overlooked in the past. In fact, we reckon that many synthesis recipes were successful because of the (unintentional) near-surface formation of silica. Note that the experiment presented in Fig. 5 is extremely surface-sensitive. The Si 2p + Cu 3p data were recorded by using a photon energy of 200 eV. At this photon energy, the Si 2p ionization cross section is more than 200-times larger than the one at the photon energy of laboratory-based XPS, pushing the detection limit to very low concentrations (see Experimental and Supplementary information).

The oxygen intercalation and reaction with Si can be detected in a dedicated *in-situ* experiment performed under UHV conditions, as shown in Fig. 6. For this purpose, we used CVD-grown graphene on a Si-loaded Cu foil which was exposed to air for 2 weeks prior to analysis. The sample was then degassed in vacuum at 80 °C for 17 h before analysis to desorb adsorbates and weakly bound intercalates. Low annealing temperature prevented Si diffusion and accumulation at the surface. Fig. 6a displays a LEEM image of the sample at this stage and reflects the typical appearance of an intact SLG film covering the Cu foil. The image shows the grain boundary of two differently faceted Cu grains exhibiting the typical morphology of g/Cu with the regular appearance of step bunches [50] (left and right side of Fig. 6a). Two pronounced, almost straight lines and a thinner, more irregular linear structure are identified as wrinkles in the CVD-grown graphene layer (see arrows). Apart from these features, the image displays no contrast and the diffraction pattern acquired by μ-LEED indicates the presence of perfectly ordered SLG on the faceted Cu support (see Supporting Information). Subsequently, the sample was annealed, and the total amount of 600 L O_2 was dosed at p (O_2) = of 1×10^{-6} mbar and temperatures ranging between 650 °C and 700 °C. After cooling down to room temperature, areas were found where oxygen intercalation under the graphene layer could be spatially

resolved. Fig. 6b displays a LEEM image of such an area where graphene wrinkles appear as broad dark lines from which medium grey patches extend towards the area of flat-lying graphene (Fig. 6b).

No contrast is observed when imaging the same region by XPEEM on the main component of the C 1s peak, evidencing that the entire Cu surface is still covered by SLG. The only contrast variation in the C 1s image appears at few collapsed wrinkles, where several graphene layers are locally stacked on top of one other, resulting in an increase of the C 1s photoelectron emission intensity (not shown). However, when tuning the kinetic energy of the photoelectron image to the low binding energy side of the C 1s peak, the XPEEM image shown in Fig. 6c evidences the same features that are resolved in the LEEM image of Fig. 6b. The photoelectron yield from the low binding energy C 1s component increases along the wrinkles and on the patches that appear slightly darker in the LEEM image. The Si 2p and O 1s images of Fig. 6d and e clearly show that the low binding energy C 1s intensity correlates with the photoelectron emission from the Si 2p and O 1s core levels. As the graphene layer remains intact, we can conclude that O_2 dosing at elevated temperatures leads to oxygen intercalation underneath the graphene layer, which attracts bulk-dissolved Si to form a silica intercalate on top of Cu. The observed contrast in the XPEEM data indicates the coverage gradient of the intercalated species. Note that especially the Si 2p and O 1s data sets suffer from a low signal-to-noise ratio indicating very low photoelectron signals and, thus, low absolute coverages of the intercalated species.

The inset in Fig. 6f indicates the regions of interest, "non-intercalated", "intercalated" and "wrinkle", from where the photoelectron spectra were extracted. Deconvolution of the local C 1s spectra clearly indicates the presence of a low binding energy component of the C 1s emission recorded from the latter two areas. The C 1s, Si 2p and O 1s spectra are compiled in Fig. 6g displaying the enhanced C 1s core level intensity at low binding energy together with an increased Si 2p and O 1s photoelectron emission signal where oxygen is intercalated and dragged Si to the surface by formation of SiO_x. Again, the Si 2p binding energy of >103 eV, together with the observed O 1s peak between 532 and 533 eV supports the assignment to intercalated silica [48,49].

As has already been stressed during the discussion of Fig. 4 and is also reported in the literature, intercalated oxygen reduces the n-doping of SLG on Cu and, thus, leads to a peak shift of the C 1s core level to lower binding energy [24]. This effect provides a sensitive indicator for oxygen intercalation which delivers the clear contrast in the C 1s image reflecting the oxygen concentration gradient caused by oxygen intercalation in the UHV experiment at 700 °C. Note that the C 1s image corresponding to the low binding energy component associated with intercalated silica does not suffer from a low signal-to-noise ratio unlike the O 1s and Si 2p data because even a low concentration of intercalated oxygen already affects the doping of the topmost graphene layer and, thus, induces the peak shift of the intense C 1s peak.

Finally, the surface coverage of the intercalated silica layer can be estimated by comparing O 1s, Si 2p and Cu 3p core level intensities taken from the 2-dimensional silica reference layer on Cu(111) indicating a silica coverage ranging between 1/4 and 1/3 of the reference phase (see Supplementary information). Despite the low signal-to-noise, the data of Fig. 6 enable us to laterally resolve the intercalation process. This occurs because the segregation of Si "fixes" the oxygen atoms to the interface between Cu and the covering SLG. As long as Si is available, the conversion of Si and O into an unreactive silica phase prevents the graphene layer from being reacted off upon high-temperature annealing at 700 °C, in contrast to the case of a Si-free Cu foil.

4. Conclusions

We have shown that the chemical and electronic properties of CVD-grown g/Cu are strongly dependent on the treatment to which the Cu foil was subjected before and during CVD synthesis. In particular, Si can be dissolved in the Cu support foil through a high-temperature treatment

in hydrogen or during CVD synthesis at $p(H_2) > 100$ mbar and T well above >1000 °C. Such Si impurities accumulate on Cu via gas-phase transport from species released from the quartz reactor wall. Since at high temperature, Si dissolves in bulk Cu, the near-surface Si concentration remains below detection limit so that the graphene growth kinetics and the crystalline quality and morphology of the resulting graphene film are not affected at all. However, the presence of dissolved Si influences the intercalation/de-intercalation processes and the formation of reactive species underneath already CVD-grown graphene to a great extent. The performed XPEEM measurements combine spatial resolution with high surface sensitivity, which is why the identified processes were not observed so far and are not reported in the literature.

When considering CVD-grown graphene on Cu foils which remain Si-free until the end of the synthesis procedure, oxygen and water readily intercalate below the grown graphene already after brief exposure to ambient conditions. Additionally, adsorbates, most likely hydrocarbons, accumulate at a slower rate on the graphene-covered Cu foil. In such cases, mild annealing below 200 °C in vacuum readily removes the adsorbates and the weakly bound intercalates. When increasing slowly the temperature to about 300 °C in vacuum, all intercalates are removed leading to perfectly crystalline graphene on a clean Cu support. Instead, long-time air exposure of Si-free g/Cu leads to the intercalation of a substantial amount of oxygen (most likely as Cu oxide). In such cases, sufficient amounts of intercalated oxygen may remain on the sample during degassing in vacuum and burn off the covering graphene layer when exceeding a sample temperature of ~320 °C.

When dealing with CVD-grown graphene on Si-loaded Cu foils on which the near-surface concentration of the dissolved silicon remains below detection limit, the intercalation/de-intercalation processes during exposure to air or during degassing in vacuum do not change at sample temperatures below ~150 °C. I.e., the quality of CVD-grown graphene and the release of intercalants during annealing is not altered in comparison to Si-free Cu foils. However, when annealing to higher temperatures, intercalating oxygen can drag Si towards the surface and form silica below the covering graphene layer. During this conversion process, Si acts as oxygen scavenger which makes graphene resistant against oxidation. This fact has been overlooked so far and might explain why certain CVD growth recipes deliver high-quality graphene, simply because silicon accumulates on the Cu foil during CVD treatment. The conversion of intercalated oxygen into intercalated silica provides not only a straightforward preparation recipe towards electronically decoupled graphene on Cu, but it can be used as well to monitor the initial stages of the intercalation process during O_2 dosing itself, which we directly observed using XPEEM.

CRediT authorship contribution statement

Tim Kratky: Writing – original draft, Validation, Investigation, Data curation, Formal analysis, Writing – review & editing. **Paul Leidinger:** Data curation, Investigation. **Patrick Zeller:** Investigation. **Jürgen Kraus:** Investigation. **Francesca Genuzio:** Investigation. **Matteo Jugovac:** Investigation. **Alessandro Sala:** Investigation. **Tevfik Onur Menteş:** Investigation, Writing – review & editing. **Andrea Locatelli:** Investigation, Writing – review & editing. **Sebastian Günther:** Writing – original draft, Visualization, Validation, Investigation, Data curation, Conceptualization, Writing – review & editing.

Declaration of competing interest

The authors declare that they have no known competing financial interests or personal relationships that could have appeared to influence the work reported in this paper.

Acknowledgements

one of us (J. Kraus).

Appendix A. Supplementary data

Supplementary data to this article can be found online at https://doi.org/10.1016/j.carbon.2024.119172.

References

[1] K.S. Novoselov, A.K. Geim, S.V. Morozov, D. Jiang, Y. Zhang, S.V. Dubonos, I. V. Grigorieva, A.A. Firsov, Electric field effect in atomically thin carbon films, Science 306 (5696) (2004) 666–669.

[2] A.K. Geim, K.S. Novoselov, The rise of graphene, Nat. Mater. 6 (3) (2007) 183–191.

[3] J. Wintterlin, M.L. Bocquet, Graphene on metal surfaces, Surf. Sci. 603 (10–12) (2009) 1841–1852.

[4] M. Batzill, The surface science of graphene: metal interfaces, CVD synthesis, nanoribbons, chemical modifications, and defects, Surf. Sci. Rep. 67 (2012) 83–115.

[5] H. Tetlow, J. Posthuma de Boer, I.J. Ford, D.D. Vvedensky, J. Coraux, L. Kantorovich, Growth of epitaxial graphene: Theory and experiment, Phys. Rep. 542 (3) (2014) 195–295.

[6] X. Li, W. Cai, J. An, S. Kim, J. Nah, D. Yang, R. Piner, A. Velamakanni, I. Jung, E. Tutuc, S.K. Banerjee, L. Colombo, R.S. Ruoff, Large-area synthesis of high-quality and uniform graphene films on copper foils, Science 324 (5932) (2009) 1312–1314.

[7] C. Mattevi, H. Kim, M. Chhowalla, A review of chemical vapour deposition of graphene on copper, J. Mater. Chem. 21 (10) (2011) 3324–3334.

[8] V.L. Nguyen, Y.H. Lee, Towards wafer-scale monocrystalline graphene growth and characterization, Small 11 (29) (2015) 3512–3528.

[9] J. Zhang, L. Lin, K. Jia, L. Sun, H. Peng, Z. Liu, Controlled growth of single-crystal graphene films, Adv. Mater. (2019) e1903266.

[10] J. Kraus, M. Böbel, S. Günther, Suppressing graphene nucleation during CVD on polycrystalline Cu by controlling the carbon content of the support foils, Carbon 96 (2016) 153–165.

[11] L. Lin, J. Li, H. Ren, A.L. Koh, N. Kang, H. Peng, H.Q. Xu, Z. Liu, Surface engineering of copper foils for growing centimeter-sized single-crystalline graphene, ACS Nano 10 (2) (2016) 2922–2929.

[12] P.H.Q. Pham, W. Zhou, N.V. Quach, J. Li, J.-G. Zheng, P.J. Burke, Controlling nucleation density while simultaneously promoting edge growth using oxygen-assisted fast synthesis of isolated large-domain graphene, Chem. Mater. 28 (18) (2016) 6511–6519.

[13] L. Brown, E.B. Lochocki, J. Avila, C.-J. Kim, Y. Ogawa, R.W. Havener, D.-K. Kim, E. J. Monkman, D.E. Shai, H.I. Wei, M.P. Levendorf, M. Asensio, K.M. Shen, J. Park, Polycrystalline graphene with single crystalline electronic structure, Nano Lett. 14 (10) (2014) 5706–5711.

[14] V.L. Nguyen, B.G. Shin, D.L. Duong, S.T. Kim, D. Perello, Y.J. Lim, Q.H. Yuan, F. Ding, H.Y. Jeong, H.S. Shin, S.M. Lee, S.H. Chae, Q.A. Vu, S.H. Lee, Y.H. Lee, Seamless stitching of graphene domains on polished copper (111) foil, Adv. Mater. 27 (8) (2015) 1376–1382.

[15] N. Reckinger, X. Tang, F. Joucken, L. Lajaunie, R. Arenal, E. Dubois, B. Hackens, L. Henrard, J.F. Colomer, Oxidation-assisted graphene heteroepitaxy on copper foil, Nanoscale 8 (44) (2016) 18751–18759.

[16] S. Jin, M. Huang, Y. Kwon, L. Zhang, B.-W. Li, S. Oh, J. Dong, D. Luo, M. Biswal, B. V. Cunning, P.V. Bakharev, I. Moon, W.J. Yoo, D.C. Camacho-Mojica, Y.-J. Kim, S. H. Lee, B. Wang, W.K. Seong, M. Saxena, F. Ding, H.-J. Shin, R.S. Ruoff, Colossal grain growth yields single-crystal metal foils by contact-free annealing, Science 362 (6418) (2018) 1021–1025.

[17] Y. Li, L. Sun, Z. Chang, H. Liu, Y. Wang, Y. Liang, B. Chen, Q. Ding, Z. Zhao, R. Wang, Y. Wei, H. Peng, L. Lin, Z. Liu, Large single-crystal Cu foils with high-index facets by strain-engineered anomalous grain growth, Adv. Mater. 32 (29) (2020) 2002034.

[18] M. Huang, M. Biswal, H.J. Park, S. Jin, D. Qu, S. Hong, Z. Zhu, L. Qiu, D. Luo, X. Liu, Z. Yang, Z. Liu, Y. Huang, H. Lim, W.J. Yoo, F. Ding, Y. Wang, Z. Lee, R. S. Ruoff, Highly oriented monolayer graphene grown on a Cu/Ni(111) alloy foil, ACS Nano 12 (6) (2018) 6117–6127.

[19] M. Wang, M. Huang, D. Luo, Y. Li, M. Choe, W.K. Seong, M. Kim, S. Jin, M. Wang, S. Chatterjee, Y. Kwon, Z. Lee, R.S. Ruoff, Single-crystal, large-area, fold-free monolayer graphene, Nature 596 (7873) (2021) 519–524.

[20] J.E. Lee, G. Ahn, J. Shim, Y.S. Lee, S. Ryu, Optical separation of mechanical strain from charge doping in graphene, Nat. Commun. 3 (2012) 1024.

[21] U. Lee, Y. Han, S. Lee, J.S. Kim, Y.H. Lee, U.J. Kim, H. Son, Time evolution studies on strain and doping of graphene grown on a copper substrate using Raman spectroscopy, ACS Nano 14 (1) (2020) 919–926.

[22] A.J. Marsden, M.-C. Asensio, J. Avila, P. Dudin, A. Barinov, P. Moras, P. M. Sheverdyaeva, T.W. White, I. Maskery, G. Costantini, N.R. Wilson, G.R. Bell, Is graphene on copper doped? Phys. Status Solidi Rapid Res. Lett. 7 (9) (2013) 643–646.

[23] P.R. Kidambi, B.C. Bayer, R. Blume, Z.-J. Wang, C. Baehtz, R.S. Weatherup, M.-G. Willinger, R. Schloegl, S. Hofmann, Observing graphene grow: catalyst–graphene interactions during scalable graphene growth on polycrystalline copper, Nano Lett. 13 (10) (2013) 4769–4778.

[24] R. Blume, P.R. Kidambi, B.C. Bayer, R.S. Weatherup, Z.J. Wang, G. Weinberg, M. G. Willinger, M. Greiner, S. Hofmann, A. Knop-Gericke, R. Schlogl, The influence of

[25] intercalated oxygen on the properties of graphene on polycrystalline Cu under various environmental conditions, Phys. Chem. Chem. Phys. 16 (47) (2014) 25989–26003.

[25] A.-Y. Lu, S.-Y. Wei, C.-Y. Wu, Y. Hernandez, T.-Y. Chen, T.-H. Liu, C.-W. Pao, F.-R. Chen, L.-J. Li, Z.-Y. Juang, Decoupling of CVD graphene by controlled oxidation of recrystallized Cu, RSC Adv. 2 (7) (2012) 3008–3013.

[26] R. Wu, L. Gan, X. Ou, Q. Zhang, Z. Luo, Detaching graphene from copper substrate by oxidation-assisted water intercalation, Carbon 98 (2016) 138–143.

[27] M. Schriver, W. Regan, W.J. Gannett, A.M. Zaniewski, M.F. Crommie, A. Zettl, Graphene as a long-term metal oxidation barrier: worse than nothing, ACS Nano 7 (7) (2013) 5763–5768.

[28] F. Zhou, Z. Li, G.J. Shenoy, L. Li, H. Liu, Enhanced room-temperature corrosion of copper in the presence of graphene, ACS Nano 7 (8) (2013) 6939–6947.

[29] S. Günther, T.O. Menteş, R. Reichelt, E. Miniussi, B. Santos, A. Baraldi, A. Locatelli, Au intercalation under epitaxial graphene on Ru(0001): the role of graphene edges, Carbon 162 (2020) 292–299.

[30] V. Boix, M. Scardamaglia, T. Gallo, G. D'Acunto, M.D. Strømsheim, F. Cavalca, S. Zhu, A. Shavorskiy, J. Schnadt, J. Knudsen, Following the kinetics of undercover catalysis with APXPS and the role of hydrogen as an intercalation promoter, ACS Catal. 12 (16) (2022) 9897–9907.

[31] G. Sfuncia, G. Nicotra, F. Giannazzo, B. Pécz, G.K. Gueorguiev, A. Kakanakova-Georgieva, 2D graphitic-like gallium nitride and other structural selectivity in confinement at the graphene/SiC interface, CrystEngComm 25 (41) (2023) 5810–5817.

[32] D.G. Sangiovanni, R. Faccio, G.K. Gueorguiev, A. Kakanakova-Georgieva, Discovering atomistic pathways for supply of metal atoms from methyl-based precursors to graphene surface, Phys. Chem. Chem. Phys. 25 (1) (2023) 829–837.

[33] S. Suzuki, T. Nagamori, Y. Matsuoka, M. Yoshimura, Threefold atmospheric-pressure annealing for suppressing graphene nucleation on copper in chemical vapor deposition, Jpn. J. Appl. Phys. 53 (9) (2014) 095101.

[34] H. Zhang, Y. Zhang, Y. Zhang, Z. Chen, P.Y. Sui, X. Ge, G. Yu, Z. Jin, X. Liu, Edge morphology evolution of graphene domains during chemical vapor deposition cooling revealed through hydrogen etching, Nanoscale 8 (7) (2016) 4145–4150.

[35] S. Kasap, H. Khaksaran, S. Celik, H. Ozkaya, C. Yanik, I.I. Kaya, Controlled growth of large area multilayer graphene on copper by chemical vapour deposition, Phys. Chem. Chem. Phys. 17 (35) (2015) 23081–23087.

[36] X. Ge, Y. Zhang, L. Chen, Y. Zheng, Z. Chen, Y. Liang, S. Hu, J. Li, Y. Sui, G. Yu, Z. Jin, X. Liu, Mechanism of SiOx particles formation during CVD graphene growth on Cu substrates, Carbon 139 (2018) 989–998.

[37] I. Ruiz, W. Wang, A. George, C.S. Ozkan, M. Ozkan, Silicon oxide contamination of graphene sheets synthesized on copper substrates via chemical vapor deposition, Adv. Sci. Eng. Med. 6 (10) (2014) 1070–1075.

[38] T. Yasunishi, Y. Takabayashi, S. Kishimoto, R. Kitaura, H. Shinohara, Y. Ohno, Origin of residual particles on transferred graphene grown by CVD, Jpn. J. Appl. Phys. 55 (8) (2016) 080305.

[39] N. Lisi, T. Dikonimos, F. Buonocore, M. Pittori, R. Mazzaro, R. Rizzoli, S. Marras, A. Capasso, Contamination-free graphene by chemical vapor deposition in quartz furnaces, Sci. Rep. 7 (1) (2017) 9927.

[40] S. Al-Kamiyani, T. Mohiuddin, Improved control in elimination of white impurities on graphene by chemical vapor deposition (CVD), AIP Adv. 8 (12) (2018) 125325.

[41] S.T. Tso, J.A. Pask, Reaction of fused silica with hydrogen gas, J. Am. Ceram. Soc. 65 (9) (1982) 457–460.

[42] P. Leidinger, S. Günther, Insight into the thermodynamics of graphene growth on copper, J. Phys. Chem. C 125 (23) (2021) 12663–12671.

[43] A. Locatelli, L. Aballe, T.O. Mentes, M. Kiskinova, E. Bauer, Photoemission electron microscopy with chemical sensitivity: SPELEEM methods and applications, Surf. Interface Anal. 38 (12–13) (2006) 1554–1557.

[44] T.O. Menteş, G. Zamborlini, A. Sala, A. Locatelli, Cathode lens spectromicroscopy: methodology and applications, Beilstein J. Nanotechnol. 5 (2014) 1873–1886.

[45] N. Srivastava, Q. Gao, M. Widom, R.M. Feenstra, S. Nie, K.F. McCarty, I. V. Vlassiouk, Low-energy electron reflectivity of graphene on copper and other substrates, Phys. Rev. B 87 (24) (2013) 245414.

[46] P. Leidinger, J. Kraus, T. Kratky, P. Zeller, T.O. Menteş, F. Genuzio, A. Locatelli, S. Günther, Toward the perfect membrane material for environmental x-ray photoelectron spectroscopy, J. Phys. D Appl. Phys. 54 (23) (2021) 234001.

[47] S. Günther, T. Kratky, J. Kraus, P. Leidinger, P. Zeller, A. Sala, F. Genuzio, M. Jugovac, T.O. Menteş, A. Locatelli, Versatile procedure for the correction of non-isochromatism in XPEEM spectroscopic imaging, Ultramicroscopy (2023) 113756.

[48] J. Xu, C. Mu, M. Chen, Structure and properties of ultrathin SiOx films on Cu(111), Langmuir 38 (37) (2022) 11414–11420.

[49] F.P.J.M. Kerkhof, J.A. Moulijn, A. Heeres, The XPS spectra of the metathesis catalyst tungsten oxide on silica gel, J. Electron. Spectrosc. Relat. Phenom. 14 (6) (1978) 453–466.

[50] J. Kraus, S. Böcklein, R. Reichelt, S. Günther, B. Santos, T.O. Mentes, A. Locatelli, Towards the perfect graphene membrane? - improvement and limits during formation of high quality graphene grown on Cu-foils, Carbon 64 (2013) 377–390.

[51] M. Scardamaglia, C. Struzzi, A. Zakharov, N. Reckinger, P. Zeller, M. Amati, L. Gregoratti, Highlighting the dynamics of graphene protection toward the oxidation of copper under operando conditions, ACS Appl. Mater. Interfaces 11 (32) (2019) 29448–29457.

[52] S.Y. Lee, N. Mettlach, N. Nguyen, Y.M. Sun, J.M. White, Copper oxide reduction through vacuum annealing, Appl. Surf. Sci. 206 (1) (2003) 102–109.

[53] Y. Iijima, N. Niimura, K. Hiraoka, Prevention of the reduction of CuO during X-ray photoelectron spectroscopy analysis, Surf. Interface Anal. 24 (3) (1996) 193–197.

[54] J. Kraus, R. Reichelt, S. Günther, L. Gregoratti, M. Amati, M. Kiskinova, A. Yulaev, I. Vlassiouk, A. Kolmakov, Photoelectron spectroscopy of wet and gaseous samples through graphene membranes, Nanoscale 6 (23) (2014) 14394–14403.

[55] A. Kolmakov, L. Gregoratti, M. Kiskinova, S. Günther, Recent approaches for bridging the pressure gap in photoelectron microspectroscopy, Top. Catal. 59 (5) (2016) 448–468.

[56] A. Apponi, D. Convertino, N. Mishra, C. Coletti, M. Iodice, F. Frasconi, F. Pilo, N. S. Blaj, D. Paoloni, I. Rago, G. De Bellis, G. Cavoto, A. Ruocco, Transmission through graphene of electrons in the 30 – 900 eV range, Carbon 216 (2024) 118502.

[57] A.P. Baddorf, J.F. Wendelken, High coverages of oxygen on Cu(110) investigated with XPS, LEED, and HREELS, Surf. Sci. 256 (3) (1991) 264–271.

[58] G. Deroubaix, P. Marcus, X-ray photoelectron spectroscopy analysis of copper and zinc oxides and sulphides, Surf. Interface Anal. 18 (1) (1992) 39–46.

[59] J.J. Navarro, S. Tosoni, J.P. Bruce, L. Chaves, M. Heyde, G. Pacchioni, B. Roldan Cuenya, Structure of a silica thin film on oxidized Cu(111): conservation of the honeycomb lattice and role of the interlayer, J. Phys. Chem. C 124 (38) (2020) 20942–20949.

[60] R. Larciprete, P. Lacovig, F. Orlando, M. Dalmiglio, L. Omiciuolo, A. Baraldi, S. Lizzit, Chemical gating of epitaxial graphene through ultrathin oxide layers, Nanoscale 7 (29) (2015) 12650–12658.